

# Performance of a Hopping Rotochute

**Eric Beyer and Mark Costello**

School of Aerospace Engineering, Georgia Institute of Technology, Atlanta, Georgia

[Received date; Accepted date] — to be inserted later

## ABSTRACT

A hybrid micro air/ground vehicle has been developed and is specifically tailored to explore interior spaces with complex terrain. The vehicle, called the hopping rotochute, maneuvers through intricate environments by hopping over or through impeding obstacles. A small coaxial rotor system provides the necessary lift while a moveable internal mass allows directional control. In addition, the low mass center and egg-like exterior shape of the body creates a means to passively reorient the vehicle to an upright attitude when in contact with the ground while protecting the rotating components. This paper examines basic flight performance of the device obtained through a validated simulation. Key parameters such as system weight, rotor speed, internal mass weight and location, as well as battery capacity are varied to explore air vehicle performance characteristics such as single hop height and range, number of hops, and total achievable range. In general, the total achievable range is increased as the internal mass weight, internal mass offset, and battery capacity are increased. For a given system, an optimum rotor speed and pulse width results in the maximum achievable total range for a single battery charge. The sensitivity of the hopping rotochute to atmospheric winds is also investigated and the ability of the device to perform trajectory shaping is shown.

## 1. INTRODUCTION

The exploration of complex environments such as caves, damaged buildings, and cluttered urban settings are difficult missions for current micro ground and air vehicles to successfully complete. Micro ground vehicles can traverse effectively through terrain with small ground obstructions, but are limited when trying to maneuver over larger obstacles or steep gradients which are commonplace in these backdrops. For example, the man-portable iRobot PackBot UGV can traverse inclines only up to 60 deg [1]. To help alleviate this limitation, many different obstacle detection and avoidance algorithms have been developed to route ground vehicles around these large obstructions [2, 3]. Unfortunately, in situations where the only available path requires surmounting a steep gully or ridge, even ground vehicles equipped with obstacle avoidance algorithms fail to succeed. On the other hand, micro air vehicles can successfully fly over objects of various sizes, but have a difficult time maneuvering through tight spaces with overhead obstacles without incidence. In addition, micro air vehicles suffer from short endurance since they must remain airborne throughout the entire mission. Sophisticated control and obstacle avoidance algorithms have been developed to aid in the navigation of these small aircraft [4, 5], but the associated endurance is still very limited [6].

The limitations of micro ground and air vehicles have led to the development of hybrid vehicles which mix ground ambulation and flight [7-13]. For example, the Scout [7, 8] and Jumping Mini-Whegs [9, 10] use wheels and/or wheel-like legs to traverse relatively smooth terrain while employing a jumping mechanism to surmount obstacles up to 35 and 22 cm high respectively. Researchers at the Jet Propulsion Laboratory (JPL) and Caltech have developed a series of hoppers based on a six-bar linkage and coil spring leg mechanism that can jump up to 1.2 m high and 3 m from its original position in the horizontal direction [11]. Another hopping robot developed at Sandia National Laboratories has self-righting capability, is driven by a chemical propulsion design, and can hop up to 1 m high and a couple of meters from its starting point [12, 13]. Although these hybrid vehicles can hop over obstacles much greater than their size, their maximum attainable altitude is still limited as is their ability to shape a trajectory once airborne.

The hopping rotochute is a new hybrid micro vehicle configuration that has been developed to robustly traverse complex environments [14]. As depicted in Figure 1, the vehicle utilizes a small coaxial rotor system which provides the necessary lift to hop the robot through and over irregular terrain. The direction of travel is controlled by a moveable internal mass which allows the vehicle to tilt toward the desired direction while on the ground and creates a pitching moment once in-flight due to the offset of the rotor thrust axis and mass center. The exterior shape and components of the vehicle are laid out in such a fashion to allow the body to passively upright itself when in ground contact while protecting rotating components during collisions. The work reported here investigates the flight performance of the hopping rotochute based the trade studies performed using an experimentally validated dynamic simulation. Section 2 presents an overview of the dynamic model and the model parameters determined during the validation process which is detailed in [15]. Key parameters influencing the flight performance, such as the total mass, rotor speed, internal mass weight and location, battery capacity, and atmospheric winds are varied and the simulation-based results are reported in Section 3. Example trajectory shaping results obtained using the dynamic model are also presented before conclusions are given.

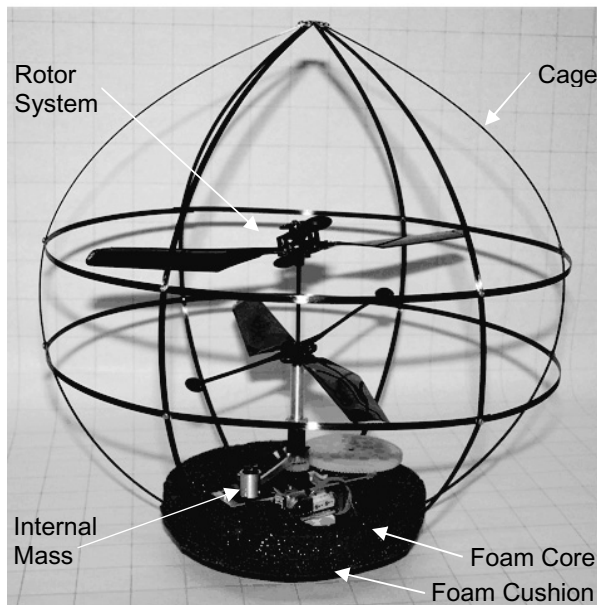


**Figure 1.** Hopping rotochute prototype

## 2. PERFORMANCE PREDICTION METHOD

The flight performance of the hopping rotochute is estimated by employing a rigid body, six degrees of freedom dynamic model which includes three inertial position components of the total mass center and three Euler orientation angles [16]. A schematic of the hopping rotochute and the reference frames used in the development of the dynamic model are shown in Figure 2, including the inertial ( $I$ ), a body ( $B$ ), and a rotor ( $R$ ) reference frame. The equations of motion describing the dynamic model of the hopping rotochute were derived and are outlined in [15]. The forces and moments embedded in the translational and rotational dynamic equations include contributions from weight, body and rotor aerodynamic loads, and contact loads. The hopping rotochute body is assumed to produce only an aerodynamic drag force at the center of pressure of the body. The aerodynamic moment contribution from the body about the mass center is caused by the offset of this drag force from the center of gravity. The rotor system produces an aerodynamic force (thrust) normal to the rotor tip path plane (frame  $R$ ) which is allowed to roll and pitch with respect to the body. As the body rotates, the rotor blades do not instantaneously follow the rotor shaft. This rotor lag is captured by employing first order filters with an associated time constant. Since the rotor aerodynamic force is not applied at the mass center, an aerodynamic moment due to the rotor system is also present. The forces and moments that act on the body during ground contact are calculated based on a soft contact model originally developed by Goyal, Pinson, and Sinden

[17, 18]. The soft contact model estimates the contact loads, including dry friction, by modeling localized non-permanent material deformation of the contacting surfaces. The exterior shape of the body is approximated with vertices, while a horizontal plane represents the ground as shown in Figure 3. Each body vertex is connected to an associated surface element (SE) through two pairs of massless springs and dampers. The ground plane also has a similar arrangement of springs and dampers as shown in Figure 3. During simulation, a collision detection method determines which body vertices are contacting the ground plane and the point of contact. The forces in the normal and tangential direction at each contact point are calculated based on the spring and damper constants as well as the spring lengths and the velocity at the contact point. The moment about the mass center from the contact loads are based on the distance vector from each contact point to the center of mass and the force at the contact point.

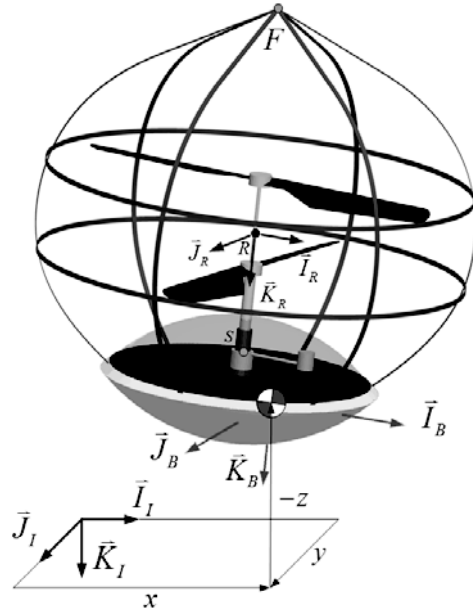


**Figure 2.** Hopping rotochute schematic

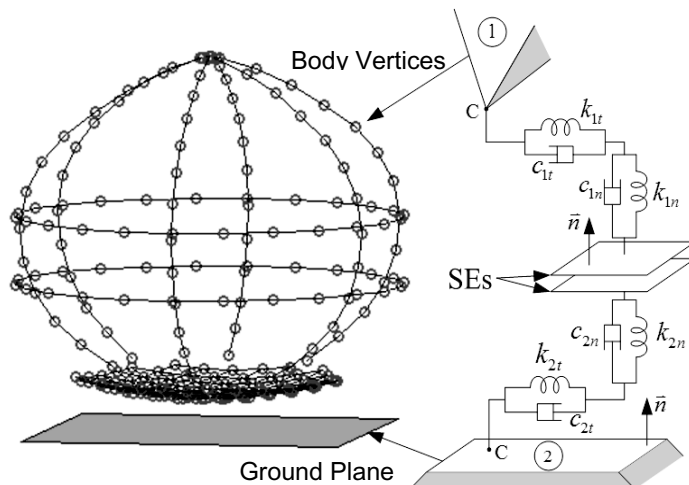


**Figure 3.** Soft contact model body vertices/ground face and spring/damper schematic

The hopping rotochute dynamic model was validated by comparing recorded data using a motion capture system [19] of a hopping rotochute prototype (Figure 1) with simulation results of the same scenario [15]. The spring and damper constants of the foam cushion on the bottom of the prototype used

in the contact model were found to be 212 N/m and 0.5 N·s/m respectively for both the normal and tangential directions based on a vertex spacing of 6.9 mm. The spring and damper constants of the ground material (carpet) were determined to be 120 N/m and 0.5 N·s/m along both directions. The coefficient of friction associated with these two materials was experimentally determined to be 3.0. The aerodynamic coefficients were calculated based on data from the motion capture system. During powered flight, the aerodynamics drag coefficient was found to be 1.0 with a center of pressure location of 16 cm along  $\vec{K}_B$  from point  $F$ . The drag coefficient and center of pressure during unpowered flight were determined to be 0.6 and 19 cm from point  $F$  along  $\vec{K}_B$ . The aerodynamic damping moment coefficients were estimated to be -0.3. The current, voltage, and power used by the motor and the corresponding thrust produced by the rotor system were experimentally obtained as a function of rotor speed and height above the ground [14]. Curves were fit to this data and subsequently used during simulation. The rotor lag time constant was experimentally determined to be 0.17 s.

### 3. FLIGHT PERFORMANCE

The hopping rotochute used in this study is based on a fabricated prototype shown in Figure 1. This vehicle consists of an expanded polypropylene (EPP) foam core, a polyurethane foam cushion, a carbon fiber cage, an internal mass, associated electronics, and a propulsion system [14]. The propulsion system from an Air Hogs Reflex Micro Helicopter was used to power the prototype and consists of a single small brushed dc electric motor, a transmission, and a coaxial rotor system. The rotor blades have a radius of 10.6 cm, a mean aerodynamic chord of 2 cm, and a pitch of about 30 deg. The internal mass is controlled by a micro servo, allowing the internal mass to rotate  $\pm 180$  deg around the internal perimeter of the body. The carbon fiber cage houses the propulsion system as well as the internal mass and was shaped to passively upright the vehicle when on the ground while protecting the rotating components. The polyurethane foam cushion helps prevent electronic damage during ground impact while damping the motion. The prototype has an overall height of 25.4 cm and a maximum horizontal cage diameter of 24.8 cm. The mass properties of the hopping rotochute without an internal mass and battery are given in Table 1. Here  $m$  is the mass of the vehicle,  $SL_{F \rightarrow CG}$ ,  $BL_{F \rightarrow CG}$ , and  $WL_{F \rightarrow CG}$  are the stationline, buttline, and waterline distances from point  $F$  to the mass center ( $CG$ ), and  $I$  represents the mass moment of inertia components. The 2-cell, 7.4 V lithium-polymer (LiPo) battery packs used to power the prototype and incorporated into this study include a 250, 300, and 480 mAh battery made by Apache, Electrify, and Thunder Power respectively. The batteries have a mass of 13.7, 19.8, and 24.6 g respectively.

Table 1. Hopping rotochute mass properties

Parameter	Value	Units
$m$	64.4	g
$SL_{F \rightarrow CG}$	0.0	cm
$BL_{F \rightarrow CG}$	0.0	cm
$WL_{F \rightarrow CG}$	17.4	g·cm <sup>2</sup>
$I_{XX}$	3069	g·cm <sup>2</sup>
$I_{XY}$	3253	g·cm <sup>2</sup>
$I_{ZZ}$	737	g·cm <sup>2</sup>
$I_{XZ}$	0	g·cm <sup>2</sup>
$I_{YZ}$	0	g·cm <sup>2</sup>

The remainder of this section is devoted to determining the flight performance of the hopping rotochute based on results obtained from the validated dynamic model described above. The dynamics of two hopping rotochute systems with different properties are first explored and used to help identify key parameters influencing the flight performance. Simulation-based trade studies are then performed to demonstrate the effects of these parameters on the flight performance. Wind sensitivity and trajectory shaping results are also given based on the dynamic model.

### 3.1 Example Trajectories

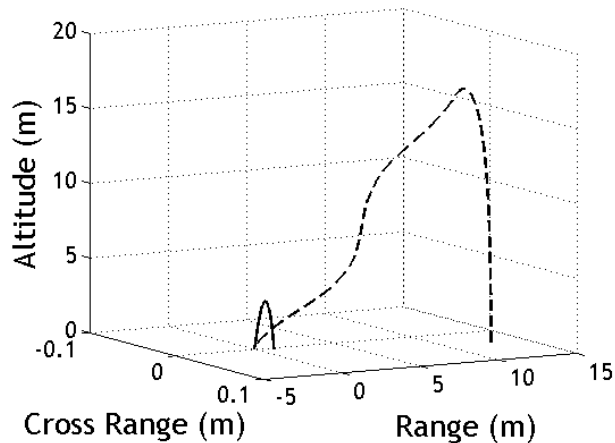
In order to determine the main flight performance drivers of the hopping rotot chute, many dynamic model simulations were performed and the resulting trajectories were compared. The results of two such example trajectories are given in Figures 4 through 12. The first trajectory, denoted with a solid line, was obtained using a system with a 300 mAh battery with an internal mass of 6 g ( $m_{IM} = 6$  g) fixed at an offset of 4 cm along  $I_B$  from point S (system 1). Note that point S is located 22 cm along  $K_B$  from point F (see Figure 2). The rotor system was powered for 1 s (pulse width = 1 s) to a speed of 4000 r/min. The second trajectory, denoted with a dashed line, is associated with a hopping rotot chute equipped with a 250 mAh battery and an internal mass of 10 g ( $m_{IM} = 10$  g) fixed at a radial location of 6 cm along  $I_B$  from point S (system 2). Here the rotor system was powered for 6 s (pulse width = 6 s) to a rotor speed of 3000 r/min. The properties of these two systems are outlined in Table 2.

Table 2. Properties of system 1 and 2

Parameter	System 1 Value	System 2 Value	Units
$m$	90.4	88.3	g
$SL_{F \rightarrow CG}$	2.65	6.80	cm
$BL_{F \rightarrow CG}$	0.0	0.0	cm
$WL_{F \rightarrow CG}$	20.6	20.4	cm
$I_{XX}$	3447	3368	$\text{g}\cdot\text{cm}^2$
$I_{YY}$	3714	3867	$\text{g}\cdot\text{cm}^2$
$I_{ZZ}$	854	1075	$\text{g}\cdot\text{cm}^2$
$I_{XY}$	0	0	$\text{g}\cdot\text{cm}^2$
$I_{XZ}$	-32	-92	$\text{g}\cdot\text{cm}^2$
$I_{YZ}$	0	0	$\text{g}\cdot\text{cm}^2$
$m_{IM}$	6	10	g
IM offset	4	6	cm
battery	300	250	mAh
pulse width	1	6	s
rotor speed	4000	3000	r/min

As shown in Figures 4 through 6, the example system time histories of the mass center position are vastly different. Since system 1 was powered for only 1 s and is heavier, due to the larger battery size, the vehicle only reached an altitude of 3.2 m while achieving a range of 0.9 m. On the other hand, system 2 is lighter and powered for a longer duration which allows the vehicle to reach an altitude of 17.4 m with a range of 11.9 m. The effects of the rotor lag time constant are also evident for system 2 causing the range time history to nearly level off at 5.5 s before more range is gained. The pitch angle associated with each trajectory is shown in Figure 7. Notice that enough time is allowed for both systems to settle to an initial launch pitch angle with values of -0.8 and -2.4 deg for system 1 and 2, respectively, before the rotor system was activated. System 2 achieves a greater initial launch angle due to the incorporation of a heavier internal mass which is located at a greater radial distance (offset). Once airborne, system 1 reaches a pitch angle of -7.6 deg before power is ceased and the moment due to the drag pitches the vehicle in the opposite direction before ground impact. The pitch angle time history associated with system 2 is more complex, pitching back and forth due to the rotor disc lag. The forward velocity time histories are shown in Figure 8. System 1 reaches a maximum forward velocity of 0.58 m/s whereas the forward velocity associated with system 2 involves damped oscillations between 0 and 2.49 m/s as the system gains altitude. Once power is shut off, the forward velocity of system 2 reaches a value of 2.86 m/s before contacting the ground. The vertical velocity of system 1, shown in Figure 9, reaches a value of -5.35 m/s when powered and hits the ground with a speed of 5.9 m/s. System 2 reaches a vertical velocity of -3.6 m/s which remains relatively constant during powered flight and contacts the ground with a vertical speed of 6.2 m/s. The rotor speed profile of both systems is shown in Figure 10. As noted earlier, system 1 is powered for 1 s with a maximum rotor speed of 4000 r/min, whereas system 2 is powered for 6 s with a maximum rotor speed of 3000 r/min. The thrust produced and power consumed is shown in Figures 11 and 12 respectively. System 1 achieves a

maximum thrust of 2.6 N at 2.33 s with an associated power of 111 W, whereas system 2 obtains maximum thrust and power at 2.25 s with values of 1.61 N and 39 W respectively. The initial peak of the thrust is due to in-ground-effect combined with high rotational speeds. By integrating the current versus time curve (not shown), the amount of energy drained from the battery during a single hop can be calculated. By dividing the battery capacity by the energy drained during a single hop, the total number of hops can be estimated. With a 300 mAh battery, system 1 is able to achieve 228 hops. With a range of 0.9 m for a single hop, system 1 is able to travel 205 m in the horizontal plane on a single battery charge. The number of hops and total range of system 2 with a 250 mAh battery is 33 and 391 m respectively.



**Figure 4.** Altitude versus cross range versus range (solid = system 1, dashed = system 2)

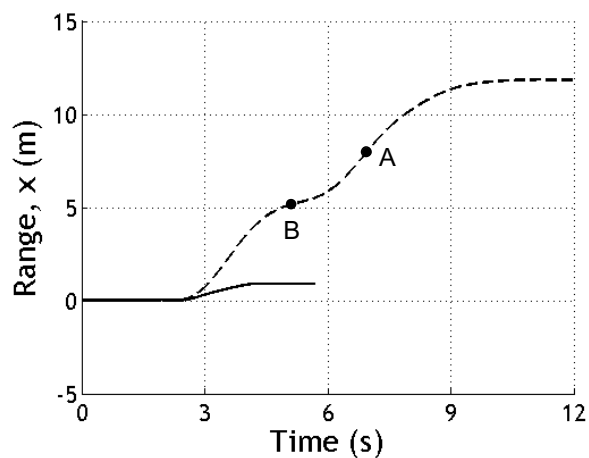


**Figure 5.** Range versus time (solid = system 1, dashed = system 2)

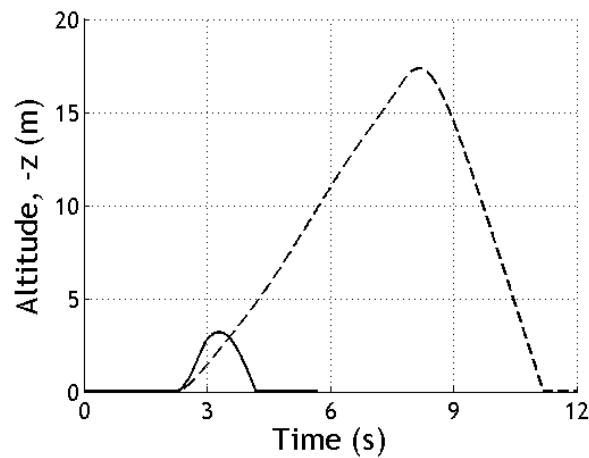


**Figure 6.** Altitude versus time (solid = system 1, dashed = system 2)

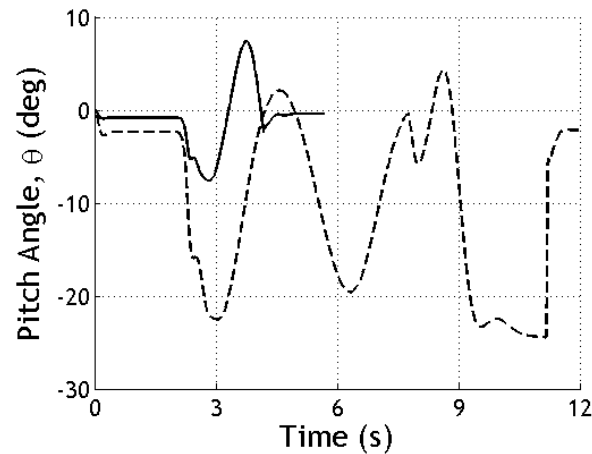


**Figure 7.** Pitch angle versus time (solid = system 1, dashed = system 2)

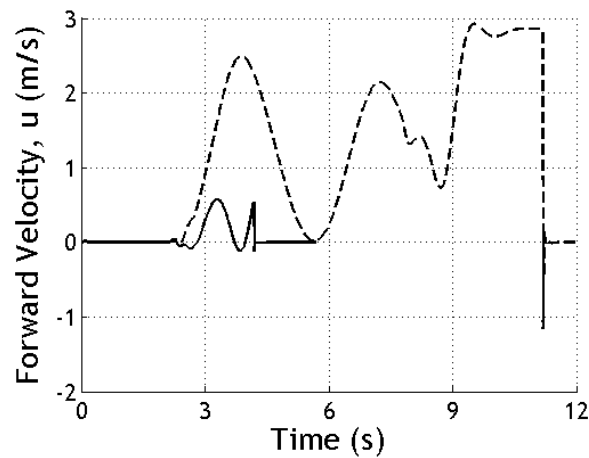


**Figure 8.** Forward velocity versus time (solid = system 1, dashed = system 2)

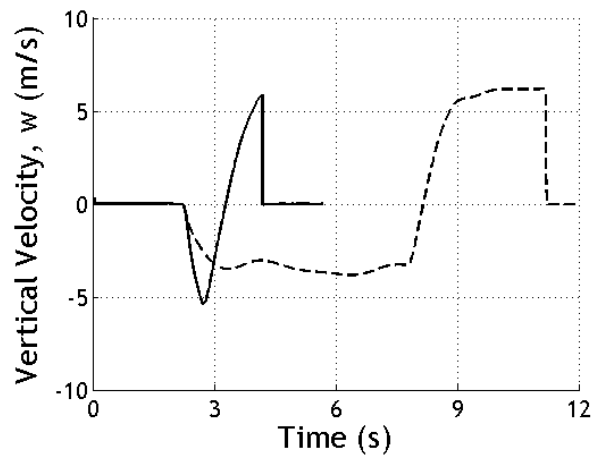


**Figure 9.** Vertical velocity versus time (solid = system 1, dashed = system 2)

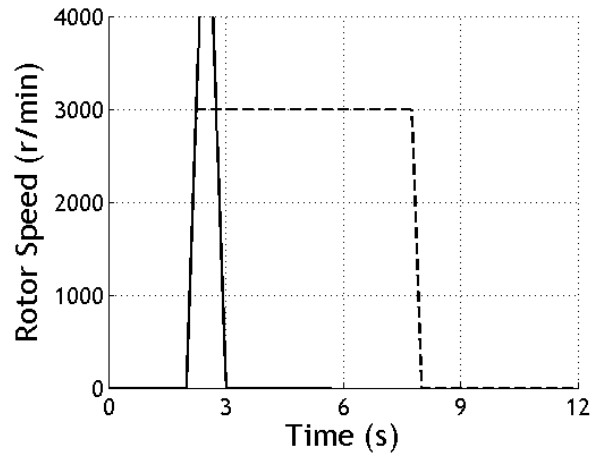


**Figure 10.** Rotor speed versus time (solid = system 1, dashed = system 2)

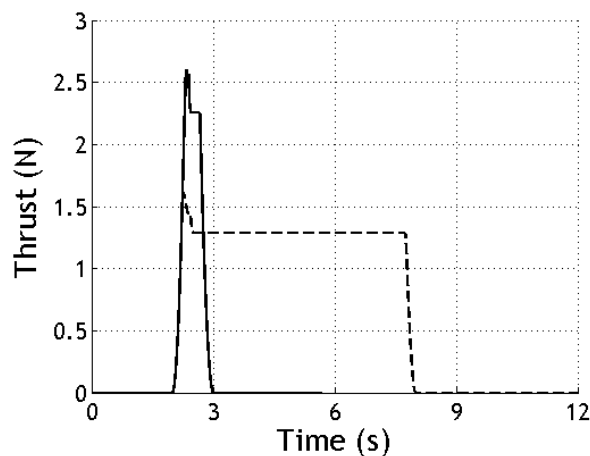


**Figure 11.** Thrust versus time (solid = system 1, dashed = system 2)

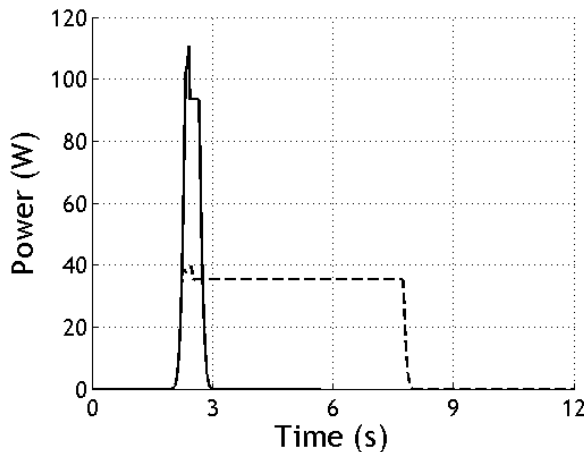


**Figure 12.** Power versus time (solid = system 1, dashed = system 2)

### 3.2 Basic Flight Performance

As demonstrated by the two example trajectories, the dynamics and flight performance of the hopping rotot chute are highly dependent on the mass properties, battery size, rotor speed profile, as well as the internal mass location and weight. To better understand how these key parameters influence flight performance, simulation-based trade studies were conducted that varied these parameters and the results are summarized below. For all trade studies, the vehicle was allowed to come to rest on the ground at its equilibrium orientation before the rotor system was activated. The rotor system was then powered for a specific amount of time (pulse width) at a given rotor speed similar to the profiles of the example trajectories. The slope of the upward and downward part of the rotor speed curve is 12,000 r/min/s and -12,000 r/min/s as is characteristic for this system [14].

For the first trade studies, time simulations were performed with different sized batteries while varying the internal mass (IM) weight and radial location (offset) as well as the rotor speed. The rotor system was powered for 1 s (pulse width = 1 s) with maximum rotor speeds which varied from 2000 to 4000 r/min in 100 r/min increments. The internal mass was varied radially from point S along  $\vec{I}_B$  in 1 cm increments from 0 to 6 cm and its mass ( $m_{IM}$ ) was varied from 0 to 10 g in 2 g increments. The total mass of the system using the 250 mAh battery and the internal mass weights previously described varied from 78.3 to 88.3 g. The total mass center location along  $\vec{I}_B$  varied from 0 to 0.68 cm depending on the internal mass weight and location. The resulting curves from this trade study associated with the 250 mAh battery system are given in Figures 13 through 17. Figure 13 presents the range achieved by a single hop as a function of internal mass offset and rotor speed. As shown, the single hop range is increased as internal mass weight and offset is increased. The increased internal mass weight and radial distance allows the body to settle at a higher initial launch pitch angle, shown in Figure 14, and also creates a larger pitching moment once airborne due to the increased moment arm between the thrust vector and center of mass of the system. Combined, these two parameters allow a slightly heavier hopping rotot chute to achieve more range during a single hop. Figure 13 also demonstrates that the single hop range increases with rotor speed. The increased rotor speed creates more thrust, allowing the vehicle to reach greater altitudes while remaining airborne for an extended period of time. The maximum altitude as a function of internal mass offset and rotor speed is shown in Figure 15. As presented, the maximum altitude varies greatly with rotor speed while the internal mass offset has little effect. The hopping rotot chute achieves a maximum altitude of 3.78, 3.68, 3.56, 3.44, 3.30, and 3.16 m with a rotor speed of 4000 r/min associated with the 0, 2, 4, 6, 8, and 10 g internal mass with no offset respectively. Figure 16 shows the total number of hops that can be achieved using a 250 mAh battery system as a function of rotor speed. As expected, more energy is consumed during flights with higher rotor speeds which reduce the number of hops. The total range that can be achieved by the hopping rotot chute with a 250 mAh battery is again calculated by multiplying the number of hops by the range of a single hop. The total range as a function of internal mass offset and rotor speed is shown in Figure 17. The total range increases as the IM weight and offset are enlarged. The total range also increases

with rotor speed up to a maximum before slightly decreasing as the rotor speed is magnified. At these higher rotor speeds, the range of a single hop increases, but more power is consumed which results in a decrease in the number of hops and a smaller total range. The maximum total range of this system with a 2, 4, 6, 8, and 10 g internal mass at a 6 cm IM offset occurs at rotor speeds of 3500, 3600, 3600, 3700, and 3800 r/min with total range values of 108, 203, 288, 369, and 435 m respectively.

Similar flight performance trends occur when the hopping rotochute is equipped with a battery of greater capacity. As shown in Figure 16, batteries with a greater capacity allow the vehicle to achieve more hops when powered for 1 s. The increased number of hops allows the system with a greater capacity to achieve a greater total range. Using a 300 mAh battery, a total range of 112, 213, 305, 393, and 468 m can be achieved with a 2, 4, 6, 8, and 10 g internal mass at an offset of 6 cm and a rotor speed of 4000 r/min respectively. These values are about 7 % higher than those achieved by the 250 mAh battery system even though the battery capacity increased by 20 %. The reason for this is the fact that the 300 mAh battery weighs 44 % more than the 250 mAh battery, creating a heavier system which achieves less altitude. The 480 mAh battery has greater capacity per weight than both the 250 and 300 mAh batteries, which allows the vehicle to attain even greater total ranges. A hopping rotochute equipped with a battery of this size is able to achieve a total range of 161, 310, 444, 571, and 683 m with a rotor speed of 4000 r/min and an IM offset of 6 cm with a 2, 4, 6, 8, and 10 g internal mass respectively.

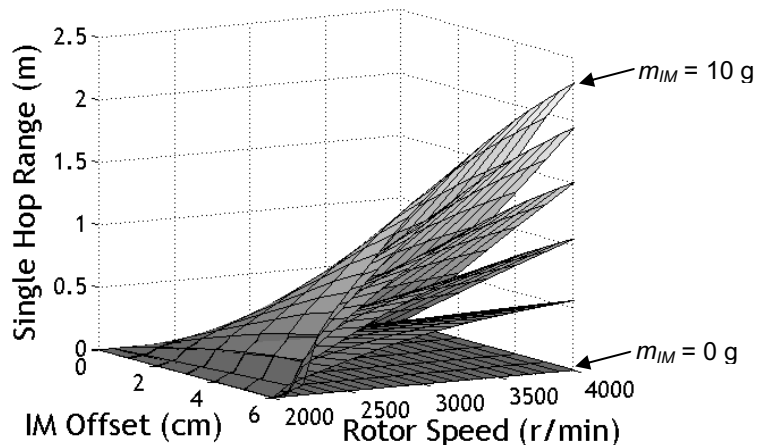


**Figure 13.** Single hop range versus internal mass (IM) offset versus rotor speed using 250 mAh battery

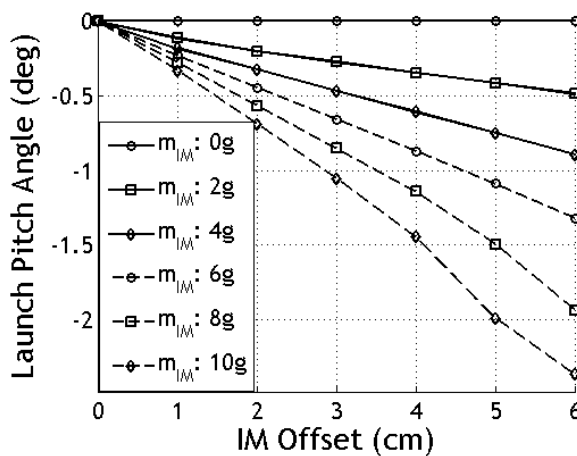


**Figure 14.** Launch pitch angle versus internal mass (IM) offset using 250 mAh battery

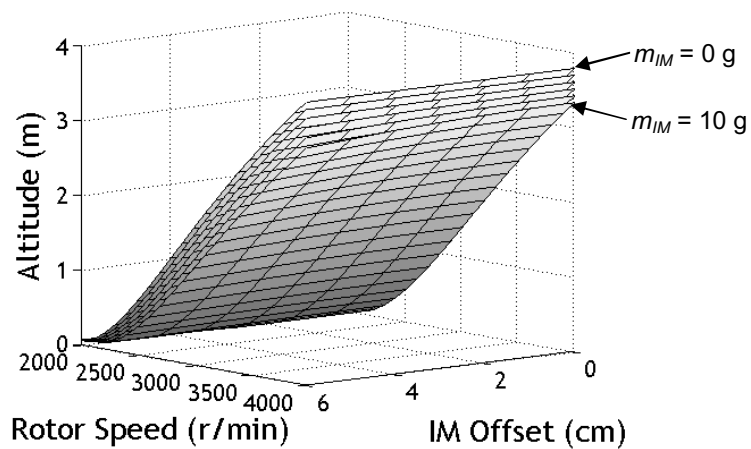


**Figure 15.** Maximum altitude versus internal mass (IM) offset versus rotor speed using 250 mAh battery

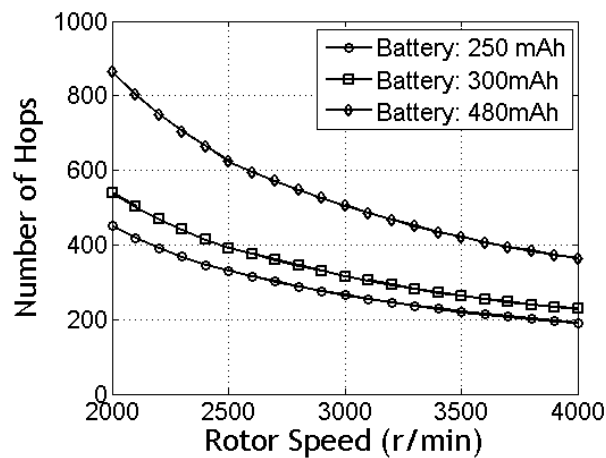


**Figure 16.** Number of hops versus rotor speed using 250, 300, and 480 mAh battery

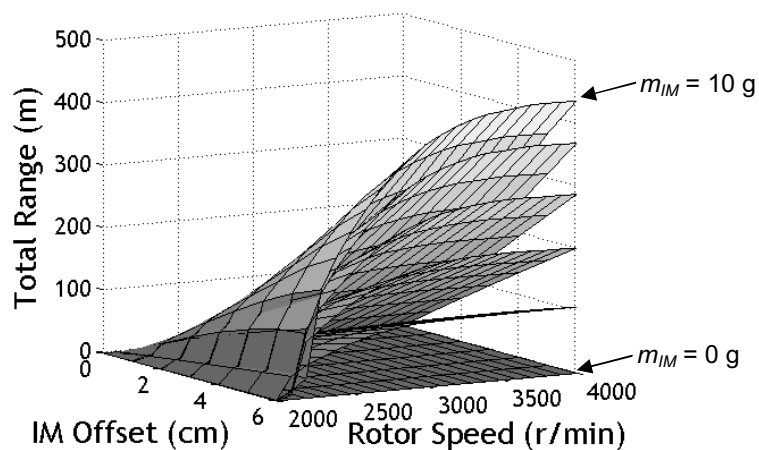


**Figure 17.** Total range versus internal mass (IM) offset versus rotor speed using 250 mAh battery

As with all micro air vehicles, the total mass of the hopping rotochute influences the flight performance of the vehicle. To better understand the effects of this parameter, the hopping rotochute mass and internal mass weight were reduced proportionally for a given internal mass offset so the mass center remained the same as the total weight decreased. The total mass of the vehicle used in this simulation-based trade study are 60, 70, 80, 90, and 100 % of those from the 250 mAh battery system with an internal mass of 6 g. This amounts to system masses of 50.6, 59, 67.4, 75.9, and 84.3 g respectively. The internal mass offset was again set to 0 through 6 cm in 1 cm increments from point  $S$  which amounts to system mass center locations along  $\bar{I}_B$  of 0, 0.07, 0.14, 0.21, 0.28, 0.36, and 0.43 cm. The results of this trade study are presented in Figure 18 which plots the total range as a function of internal mass offset and rotor speed. As shown, the maximum total range for the 60, 70, 80, 90, and 100 % mass vehicles occurs with a 6 cm IM offset at rotor speeds of 2300, 2600, 3000, 3400, and 3600 r/min respectively. The total range achieved at these rotor speeds are 378, 348, 323, 303, and 288 m. Hence, decreasing the total mass by 10, 20, 30, and 40 % increases the total range by 5, 12, 21, and 31 % respectively. Once again, these optimum values occur due to the fact that the range of a single hop increases and the number of hops decreases as the rotor speed is increased. The optimum occurs when the product of these two values are maximized. Greater altitudes are also achieved with lighter systems with smaller internal mass offsets and larger rotor speeds.

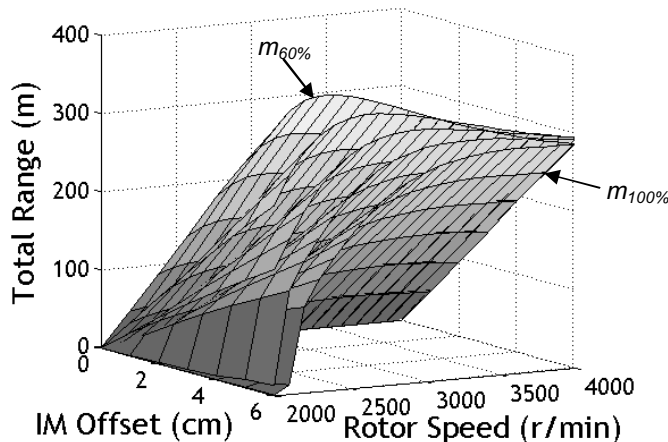


**Figure 18.** Total range versus internal mass (IM) offset versus rotor speed using 250 mAh battery

The trade studies presented above are based on powering the rotor system for 1 s at various rotor speeds. As the second example trajectory demonstrated, greater range and altitude can be achieved if the rotor system is activated for a longer period of time. To show the effects of this parameter, another simulation-based trade study was performed which varied the pulse width and rotor speed for a 250 mAh battery system with a 2, 4, 6, 8, and 10 g internal mass located at an offset of 6 cm along  $\bar{I}_B$ . The results of this trade study are shown in Figures 19 through 22. As shown in Figure 19, the number of hops exponentially decreases as the pulse width increases. The number of hops as well as the dynamics of the different weighted systems affects the total range as shown in Figure 20. Notice that the total range peaks at a pulse width of 2 s and a rotor speed of 2600 r/min. Increasing the rotor speed and pulse width from this peak tend to decrease the total range although smaller amplitude peaks occur when the pulse width is 5 and 8 s. The peaks and troughs that occur as the pulse width is varied are caused by the dynamics of the system. As shown by the second example trajectory, the rotor lag causes the slope of the range versus time curve to vary. The peaks in the total range curves of Figure 20 occur when the power is ceased while the slope is steep, as demonstrated by point  $A$  in Figure 5. The troughs occur when the power is shut off while the slope of the range versus time curve is small, see point  $B$  in Figure 5. The maximum altitude as a function of pulse width and rotor speed is shown in Figure 21. As one would expect, the maximum altitude increases as the rotor speed and pulse width are increased. Figure 22 plots the total range as a function of altitude for the systems using a 2, 4, 6, 8, and 10 g internal mass while powered for 2 s. As shown, the maximum total range associated with each IM weight peaks at around 2 m of altitude and decreases as the altitude increases. Similar trends occur when the pulse width is increased, with greater altitudes being attained.

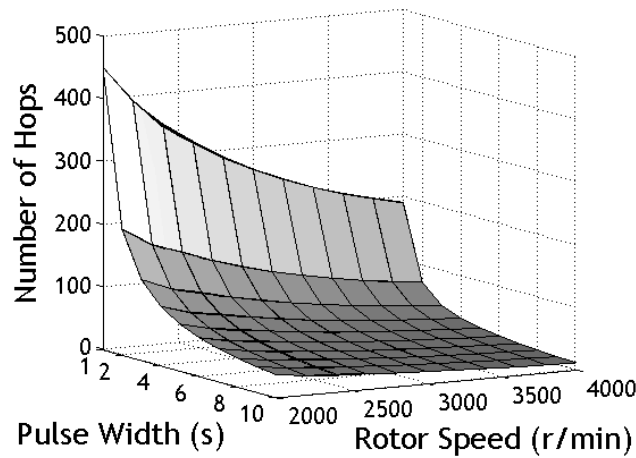


**Figure 19.** Number of hops versus pulse width versus rotor speed using 250 mAh battery

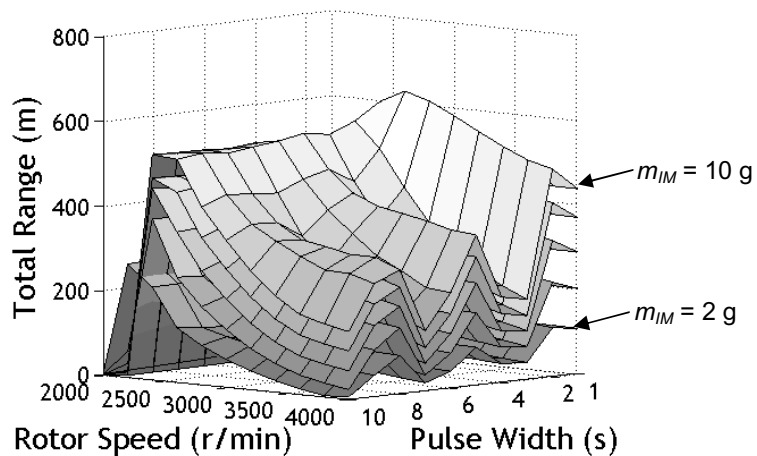


**Figure 20.** Total range versus pulse width versus rotor speed using 250 mAh battery

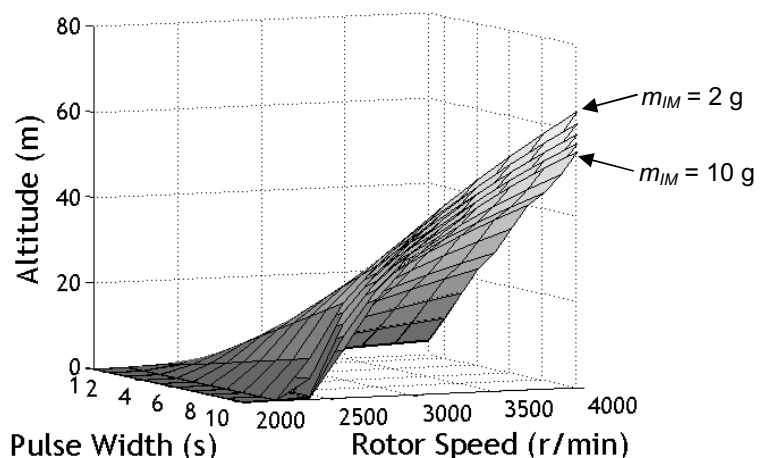


**Figure 21.** Maximum altitude versus pulse width versus rotor speed using 250 mAh battery

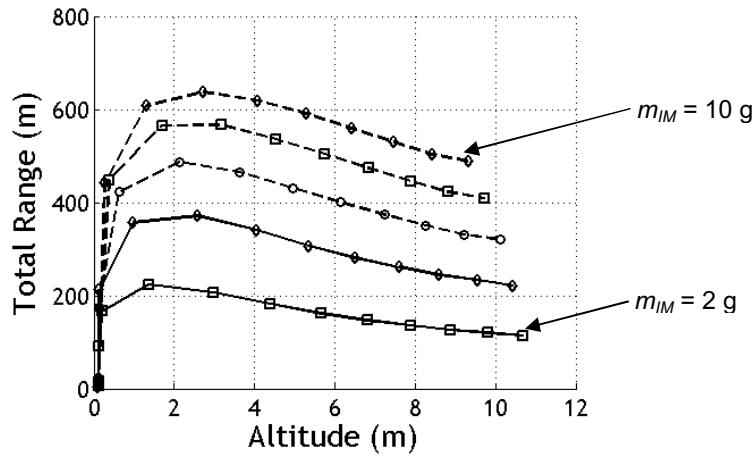


**Figure 22.** Total range versus maximum altitude with 2 s pulse width using 250 mAh battery

### 3.3 Atmospheric Wind Sensitivity

In order to robustly traverse complex terrain, a cage was built around the rotor system to protect the rotating components. Unfortunately, this structure and the base of the vehicle create additional drag which impedes the motion of the vehicle while airborne. In order to determine how well the hopping rotochute performs with typical atmospheric winds acting upon it, simulation-based trade studies were performed to predict wind sensitivity of the vehicle. For the first wind trade study, atmospheric winds of various speed and direction within the horizontal plane were applied to a hopping rotochute with a 250 mAh battery and a 10 g internal mass at a 6 cm offset along  $I_B$ . The vehicle was initially positioned at the origin with the  $I_B$  axis directed toward the  $I_I$  axis while the rotor system was powered for 1 s to a rotor speed of 4000 r/min. The wind speed ( $V_{MW}$ ) was varied between 0.25 and 1.5 m/s in 0.25 m/s increments at azimuthal angles of 0 to 350 deg in 10 deg increments. The results of this analysis are given in Figure 23. As shown, the wind dispersion plot for a given wind magnitude is elliptical in nature with higher winds giving higher dispersion radii. Also note that for this particular system, head wind speeds above 1.20 m/s allow the vehicle to land behind where it initially started. Similar trends occur when using a similar system with an internal mass of 0, 2, 4, 6, and 8 g at an offset of 6 cm. A head wind with a magnitude of 0, 0.33, 0.59, 0.82, and 1.02 m/s allow a vehicle with an internal mass of 0, 2, 4, 6, 8 g to land in the same position as it began.

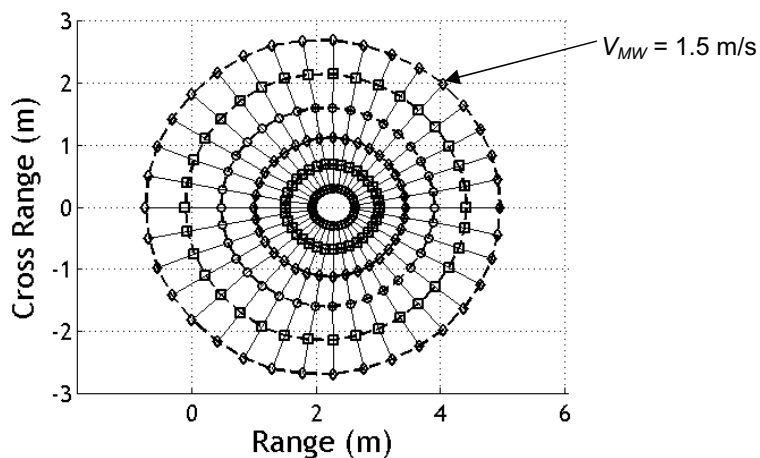


**Figure 23.** Wind dispersion

### 3.4 Trajectory Shaping

Using the rotor speed and internal mass location as inputs, the trajectory of the hopping rotot chute can also be dramatically shaped. Two such shaped trajectories are shown in Figure 24. For both simulations, the goal was to fly around a 10 m diameter cylinder that is 5 m high using a 6 g internal mass located 6 cm from the pivot point  $S$ . During the first trajectory, shown with the solid line, the internal mass is allowed to rotate around the internal perimeter of the base about the  $\vec{K}_B$  axis by an angle  $\psi_{IM}$  from the  $\vec{I}_B$  axis. As shown in Figure 24, the hopping rotot chute is able to fly around the back side of the cylinder using the rotor speed and IM azimuth angle time histories presented in Figures 25 and 26 respectively. The second trajectory, denoted by the dashed line, hops over the cylinder by employing an internal mass which can rotate about the  $\vec{J}_B$  axis by an angle  $\theta_{IM}$  from the  $\vec{I}_B$  axis. As shown in Figure 24, the vehicle initially reaches an altitude of about 4 m before the internal mass is pitched forward allowing the vehicle to fly over the cylinder. The rotor speed and internal mass pitch angle time histories for this trajectory are also shown in Figures 25 and 26 respectively.

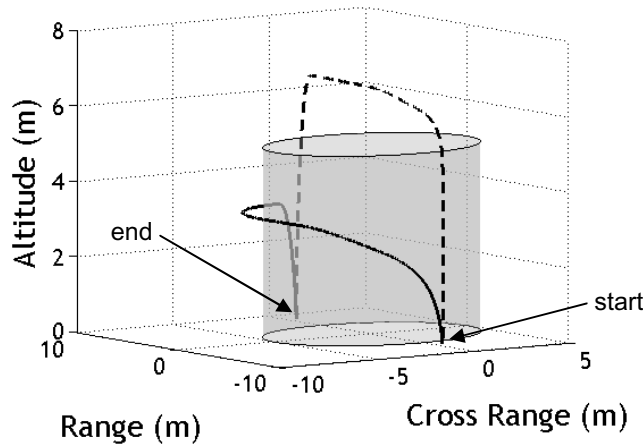


**Figure 24.** Altitude versus cross range versus range during trajectory shaping

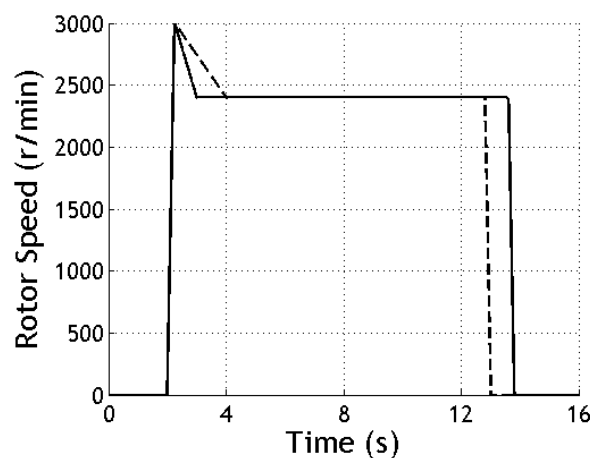


**Figure 25.** Rotor speed versus time during trajectory shaping

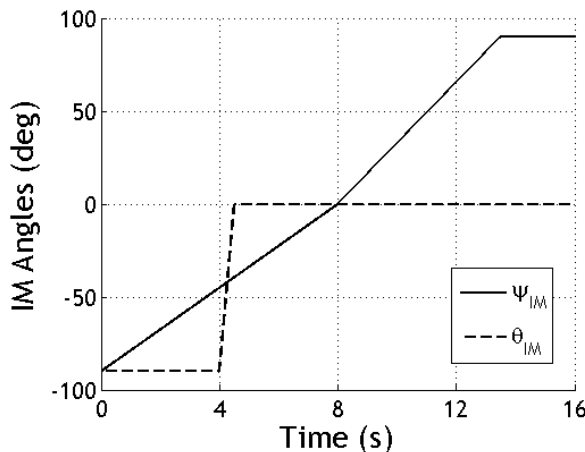


**Figure 26.** Internal mass (IM) angle versus time during trajectory shaping

#### 4. CONCLUSION

The hopping rotochute is a promising new hybrid ground/air vehicle that was specifically designed to robustly traverse difficult environments such as caves and damaged buildings. The exterior shape as well as the low mass center allow the hopping rotochute to always upright itself once on the ground, a feature that most current micro air vehicles are lacking. The internal mass, which is able to rotate around the perimeter of the base, allows the vehicle to hop in any given direction over obstacles which hamper typical ground vehicles. Due to the hopping method of mobility, the vehicle only uses substantial power when the rotor is powered during a hop. Once in a desired location, the aircraft requires minimal power, so in this sense the vehicle has much longer endurance, compared to conventional micro air vehicles. The work reported here focused on basic flight performance of the hopping rotochute. Through the employment of a validated dynamic simulation model, trade studies show that key parameters influencing flight performance include total system mass, rotor speed profile, internal mass weight and location, as well as battery capacity. In general, the total achievable range of the device can be increased by incorporating a larger internal mass at an increased radial offset which effectively magnifies the initial launch pitch angle and creates a larger pitching moment once airborne. Minimizing the weight of the total system will also increase the total range as does using a battery with a high capacity per weight ratio. The total range of the vehicle can be optimized based on maximizing the product of the number of hops and the range of a single hop of a given system. The maximum total range is also dependent on the pulse width and the dynamics of the system. Due to the relatively large coefficient of drag associated with the body, moderate atmospheric winds can offset the range achieved during a single hop. By using the internal mass as a directional control mechanism, the trajectory of the hopping rotochute can be shaped to maneuver the vehicle around large, intricate objects.

#### REFERENCES

- [1] Yamauchi, B., Daredevil: Ultra-Wide Radar Sensing for Small UGVs, *Proceedings of SPIE (vol. 6561): Unmanned Systems Technology IX*, Orlando, FL, 2007.
- [2] Borenstein, J. and Koren, Y., Real-time Obstacle Avoidance for Fast Mobile Robots, *IEEE Transactions on Systems, Man, and Cybernetics*, 1989, 19(5), 1179–1187.
- [3] Lorigo, L.M., Brooks, R.A., and Grimson W.E.L., Visually-Guided Obstacle Avoidance in Unstructured Environments, *Proceedings of the 1997 IEEE/RSJ International Conference on Intelligent Robots and Systems (vol. 1)*, Grenoble, France, 1997, 373–379.
- [4] Ollero, A. and Merino L., Control and Perception Techniques for Aerial Robots, *Annual Reviews in Control*, 2004, 28(2), 167–178.
- [5] Call, B., Beard, R., Taylor, C., and Barber B., Obstacle Avoidance for Unmanned Air Vehicles using Image Feature Tracking, *AIAA Guidance, Navigation, and Control Conference and Exhibit*, Keystone, CO, 2006, AIAA Paper 2006-6541.

- [6] Galinski, C. and Zbikowski, R., Some Problems of Micro Air Vehicles Development, *Bulletin of the Polish Academy of Sciences: Technical Sciences*, 2007, 55(1), 2279–2804.
- [7] Stoeter, S.A., Rybski, P.E., Gini, M., and Papanikolopoulos, N., Autonomous Stair-Hopping with Scout Robots, *Proceedings of the 2002 IEEE/RSJ International Conference on Intelligent Robots and Systems (vol. 1)*, Lausanne, Switzerland, 2002, 721–726.
- [8] Drenner, A., Burt, I., Dahlin, T., Kratochvil, B., McMillen, C., Nelson, B., Papanikolopoulos, N., Rybski, P., Stubbs, K., Waletzko, D., and Yesin, K.B., Mobility Enhancements to the Scout Robot Platform, *Proceedings of the 2002 IEEE International Conference on Robotics and Automation (vol. 1)*, Washington D.C., 2002, 1069–1074.
- [9] Morrey, J.M., Lambrecht, B., Horchler, A.D., Ritzman, R.E., and Quinn, R.D., Highly Mobile and Robust Small Quadruped Robots, *Proceedings of the 2003 IEEE International Conference on Intelligent Robots and Systems (vol. 1)*, Las Vegas, NV, 2003, 82-87.
- [10] Horchler, A.D., Quinn, R.D., Lambrecht, B., and Morrey, J.M., Highly Mobile Robots that Run and Jump, U.S. Patent 7249640, 2007.
- [11] Fiorini, P. and Burdick, J., The Development of Hopping Capabilities for Small Robots, *Autonomous Robots*, 2003, 14(2-3), 239–254.
- [12] Spletzer, B.L., Fischer, G.J., Marron, L.C., Martinez, M.A., Kuehl, M.A., and Feddema, J.T., Hopping Robot, U.S. Patent 6247546, 2001.
- [13] Weiss, P., Hop...Hop...Hopbots!: Designers of Small, Mobile Robots takes Cues from Grasshoppers and Frogs, *Science News*, 2001, 159(6), 88–90.
- [14] Beyer, E. and Costello, M., Design and Testing of a Hybrid Micro Vehicle – The Hopping Rotochute, *IEEE/ASME Transactions on Mechatronics*, submitted for publication, 2009.
- [15] Beyer, E. and Costello, M., Measured and Simulated Motion of a Hopping Rotochute, *Journal of Guidance, Control, and Dynamics*, accepted for publication, 2009.
- [16] Etkin, B., *Dynamics of Atmospheric Flight*, Dover, New York, NY, 2000, 121–152.
- [17] Goyal, S., Pinson, E.N., and Sinden, F.W., Simulation of Dynamics of Interacting Rigid Bodies Including Friction I: General Problem and Contact Model, *Engineering with Computers*, 1994, 10, 162–174.
- [18] Goyal, S., Pinson, E.N., and Sinden, F.W., Simulation of Dynamics of Interacting Rigid Bodies Including Friction II: System Design and Implementation, *Engineering with Computers*, 1994, 10, 175–195.
- [19] VICON System Reference, VICON Motion Systems Limited, Oxford, UK, 2007.